Comparison of LOX/Methane and LOX/Hydrogen cryogenic spray combustion with simultaneous optical diagnostics

N. Fdida, L. Vingert*, Y. Mauriot*, L.H. Dorey* and M. Théron***

ONERA – The French Aerospace Lab, 91761, Palaiseau, France
nicolas.fdida@onera.fr
***CNES – Launcher Directorate, 52 rue Jacques Hillairet, 75012, Paris, France*
marie.theron@cnes.fr

Abstract

ONERA and CNES are collaborating to prepare the next engine generation for reusable launchers that will use liquid oxygen (LOX) and methane (CH4) as propellants. The present experimental study was carried out on the MASCOTTE test bench located at ONERA, Palaiseau center. The main goal was to characterize the LOX jet, under reacting conditions, with simultaneous droplet-size measurements and high-speed chemiluminescence and shadowgraphy visualizations for two propellant couples: LOX/CH4 and LOX/H2, under similar operating conditions. High-speed visualizations were used to assign the locations of drop-size measurements obtained in the cryogenic jet flames, to explain the results and to analyse the peculiarities of combustions with both propellants.

1. Introduction

ONERA and CNES are working together to support the preparation of the next generation of engines for reusable launchers that will be propelled by liquid oxygen (LOX) and methane (CH4). The use of methane has many advantages: it is less expensive, easier to handle and liquid at a temperature close to that of oxygen. Moreover, methane can be stored in more compact tanks, as CH4 is six times denser than hydrogen, and makes the engine potentially easier to recover for reuse. In this context, ONERA and CNES have a common interest to study the methane cryogenic combustion.

The design of next engine generation will be based on high fidelity numerical simulations that will have to predict, as closely as possible, the operating conditions within the combustion chamber. At present, the current LOX/H2 injection system is still a challenge to model, especially in low thrust engine operating conditions where the oxygen jet is a two-phase flow. The droplet sizes of the LOX spray, usually characterized by a probability density function [1], are important data for validation or initialization of combustion numerical simulations. Those data will be used for the models that are developed at ONERA to predict the atomization of the continuous liquid phase and the production of the dispersed phase [2].

In order to provide input or validation data for the numerical models developed at ONERA, this experiment is conducted at the reference operating point A-10 defined by the work of the research group "combustion in rocket engines" [3]. A phase-Doppler interferometer (PDI) is used to characterize the droplet sizes of the LOX spray, atomized by the high-speed fuel gas. To provide adequate data for the models and simulations, the PDI measurement volume was positioned as close as possible to the LOX jet, in the primary atomization zone, that is near the LOX post exit. Thus the PDI measurements are located at $x/DL \leq 10$, DL being the LOX post diameter and x the injection axis. In the past, droplet-size measurements of such cryogenic LOX/H2 flames were performed at ONERA, in the same A-10 operating conditions, by Gicquel and Vingert [4] with a PDPA (Phase Doppler Particle Analyzer) and by Fdida et al. [5], withsim jet imaging. The originality of this study consists in performing droplet-size measurements closer to the LOX post and also in a LOX/CH4 cryogenic flame, in order to measure the droplet sizes produced by the primary atomization process. Moreover, high-speed shadowgraphy is run simultaneously to PDI to visualize the spray location and the dynamics of LOX droplets with a close field of view. Before presenting the PDI measurements, large field visualizations are presented for both flame test cases (LOX with H2 or CH4). Firstly, images of chemiluminescence of the OH* radical are presented to show the flame front position. Secondly, large field shadowgraphs are used to determine the whole LOX jet topology and to visualize the droplets location. These

N. Fdida, L. Vingert, Y. Mauriot, L.H. Dorey, M. Théron

visualisations are essential to explain the differences observed between these two reactive test-cases and between the validation rates of the PDI, as a function of the position of the measurement volume in the flame.

2. Experimental setup

2.1 The High Frequency Box (BHF)

For this experimental test campaign, the BHF combustion chamber was used on the MASCOTTE test bench, located at ONERA Palaiseau center. The optical setup and the combustion chamber are shown on Figure 1.The BHF was initially designed for high-frequency instability studies for rocket engine applications [6]. The BHF benefits of large optical accesses, allowing to visualize several injectors that can be mounted inside the test chamber. In this study, only one injector is mounted inside the chamber, the other injection exits being blocked. The advantage of this combustion chamber for PDI is the large optical accesses which are essential to perform droplet size measurements close to the injector exit. The combustion chamber was fed with gaseous hydrogen and liquid oxygen through a single coaxial injector. The injector was constituted of a central tube fed with oxygen and a coaxial outer tube fed with hydrogen or methane.
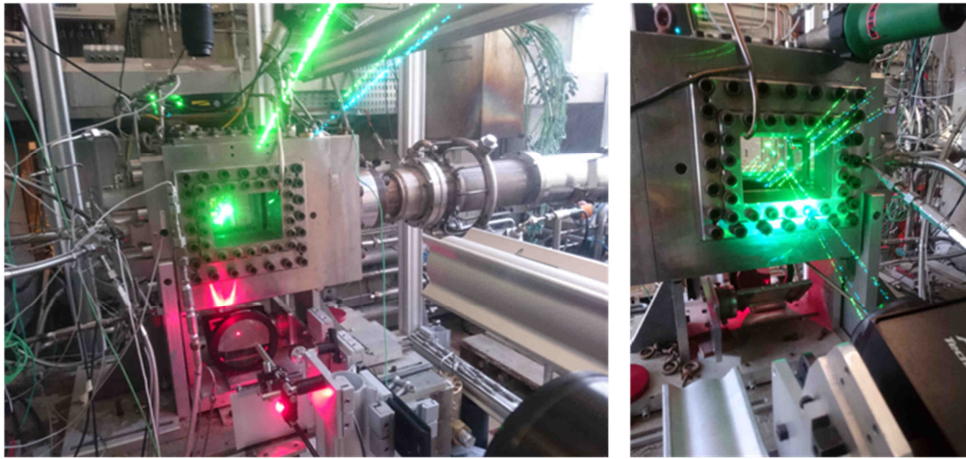
Figure 1: Illustrations of the optical setup from both sides of the MASCOTTE test bench

The operating conditions for the LOX/H2 combustion are the A-10 reference conditions [3], which already had a large existing database, except for droplet-size close from the injector. The effective chamber pressure was 0.95 MPa, the mixing ratio was ROF ≈2.3, and the momentum flux ratio J was ≈13.4. The mixing ratio ROF is defined here as the ratio between the LOX flowrate to the hydrogen flowrate and the momentum flux ratio J stands for the gas-to-liquid momentum flux ratio. Considering the oxygen critical pressure $Pc(O2) = 5.04$ MPa and temperature $Tc(O2) = 154.6$ K, LOX was injected in the combustion chamber in subcritical conditions, that is at a pressure and a temperature below the oxygen critical conditions. Those subcritical conditions are suited to study atomization of such a spray, because when $Pc > Pc(O2)$, the injection becomes supercritical and the dense oxidizer elements cannot be clearly distinguished from their surrounding medium. The gaseous Weber number We based on the LOX post diameter is about 2.10^4 and the liquid Reynolds number based on the LOX post diameter DL is Re ≈ 6.10^4. These dimensionless numbers values are representative of a rocket engine injection system [7]. Lasheras and Hopfinger [7] proposed a classification of coaxial jet breakup regimes as a function of three parameters, We, Re, and the momentum flux ratio J. In our study, the jet atomization can be considered as a fiber-type breakup. This regime is characterized by the creation of very thin and short liquid fibers created from the continuous liquid jet exiting from the nozzle. These fibers are rapidly peeled off the jet and stretched by the differential velocity between the liquid jet and the outer gas stream, from which the Weber number depends. The characteristic break-up time is very short, which means a rapid atomization of the majority of the liquid. The droplets produced have very small sizes, several orders of magnitude smaller than the injection diameter. High speed imaging is then necessary to capture the spray dynamics and the PDI is used to measure the droplet sizes and velocities created as soon as the liquid exits from the LOX post. To illustrate this phenomenon, a pair of instantaneous images is presented on Figure 2.
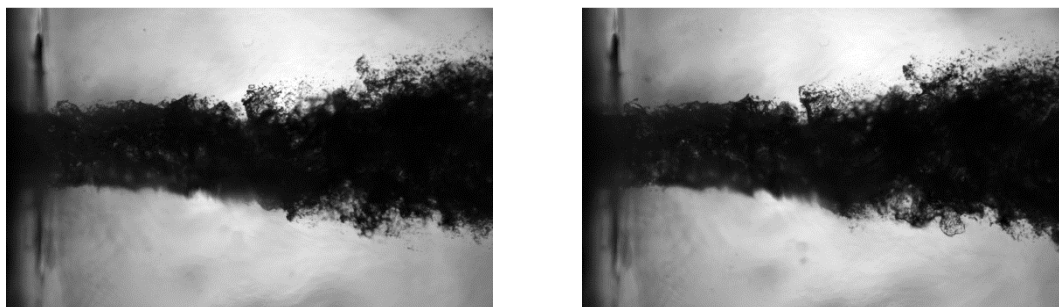
Figure 2: Instantaneous image pair of the LOX/H2 flame, recorded at 7.5 kHz in the A-10 conditions [6]

In the case of the LOX/CH4 cryogenic jet flame, there is a lack of data concerning the atomization of the LOX jet under reacting conditions [8]. The choice for the operating conditions with methane results from a compromise between the industrial needs (operating conditions at low thrust should be in subcritical conditions), the optical configuration (similar optical setup and limited soot production) and the test bench equipment available. Thus, the pressure in the combustion chamber for LOX/CH4 combustion is almost the same than in LOX/hydrogen (0.94 MPa) and the momentum flux ratio is J=21.

Three optical diagnostics were implemented simultaneously around the MASCOTTE test bench: firstly OH* chemiluminescence was synchronized with high-speed shadowgraphy to visualize the jet flame in a large field of view. This first phase is essential to locate the PDI measurement points in order to collect a large number of droplets during the stationary phase of the flow, which duration is about 30 s. Secondly, Phase Doppler interferometry was combined with high-speed shadowgraphy with a close field of view.

2.2 Imaging setup

Two complementary imaging systems were set with a large field of view, in order to see the LOX jet and the flame locations synchronously. Shadowgraphy consists in taking pictures of the illuminated liquid jet by a light source located opposite to the camera (see Figure 3). In order to visualize the dynamics of the liquid oxygen jet at the LOX post exit, a high-speed Phantom v711 camera from Vision Research was used. It is equipped with a CMOS sensor of 1280 x 800 pixels of 20 microns side. This 12-bit monochrome camera records the signal on 4096 gray levels, with an active sensor size of 1280 x 720 pix² and a frame frequency set at 1kHz. A 105 mm fixed focal length is set on the camera with an aperture of f/5.6. The resulting resolution is about 10 pix/mm. A filter is mounted on the lens of the camera to select only the light from the backlight and remove visible flame emission. The light source is a Cavilux Smart pulsed laser source [9] emitting in the red at 648 nm.

Chemiluminescence imaging was operated simultaneoulsy to visualize the flame reaction zone. The reaction mechanisms involved in combustion processes are numerous and complex. They consist of a large number of elementary reactions involving generally free radicals and molecules. In the combustion zone, elemental reactions produce radicals directly on excited energy levels. These species, that are out of thermodynamic equilibrium, relax spontaneously and almost instantaneously by emitting a photon characteristic of a transition energy to a lower level. This resulting light emission, which is characteristic of spontaneous radiative relaxation of species chemically created on excited states, such as the excited OH radical, denoted OH*, is called chemiluminescence. As soon as there is simultaneous presence of hydrogen and oxygen atoms in a flame, it is possible to detect the emission of the OH* spectrum. Such an emission spectrum was presented by Mayer et al. [10] in a rocket engine application with LOX and H2 as propellants. The signature of OH* radical is identified by the peak at 320 nm. Indeed, this transition emits light in the ultraviolet domain (UV), mainly in the spectral band 300-325 nm. This radical is emitted in the reaction zone of the flame; it is therefore particularly interesting to use it as a tracer of the chemical reaction zone, keeping nevertheless in mind that self absorption of OH* can have a non negligible impact on the interpretation of OH* images [11].

In the case of LOX/CH4 cryogenic jet flames, few data are available in the literature. Thus, the emission spectrum of the flame was recorded between 188 nm and 860 nm with an Ocean Optics S2000 spectrometer, with a resolution of 0.37 nm and an exposure time of about 100 ms. Light coming from the flame was collected by a lens focused on the flame axis, approximately in the middle of the window section. Flame emission spectroscopy was used to identify the most emitting chemical species for each operating condition. Figure 3 shows the emission spectra of the flame for two pressure conditions (0.45 MPa and 0.9 MPa in red and blue respectively).

The emission spectra of the flame are consistent with the results of Lux and Haidn [12] who also studied the emission spectrum of high-pressure LOX/CH4 flames. The intense emission peak observed around 310 nm is due to the presence of OH radical whereas the other high intensity peak around 430 nm is due to another radical, CH. Both

N. Fdida, L. Vingert, Y. Mauriot, L.H. Dorey, M. Théron

radicals are known to be produced by combustion in the chemical reaction zone. Other species, such as C2, known to be a soot precursor, can be identified by several small peaks, called Swan bands, in the case of the 0.45 MPa spectrum only. In the case of the 0.9 MPa spectrum, the continuous emission background, between 350 nm and 650 nm, which can be attributed to larger molecules such as CO_2, is too intense to see the Swan bands in this operating condition. In both pressure cases, OH and CH are intense enough to come out from the background and can thus be used as markers of the reaction zone for imaging purpose.
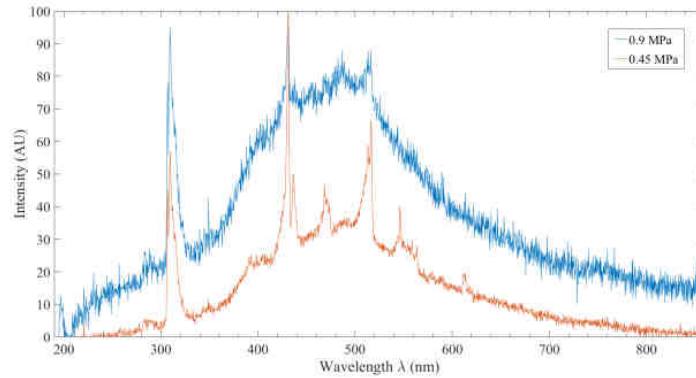
Figure 3: Emission spectra of the LOX/CH4 flame.

In order to visualize the reaction zone with OH* chemiluminescence, a UV imaging system was set up on the MASCOTTE bench (see Figure 4). It consists of an intensified high-speed camera (Photron FASTCAM Ultima APX I²), with a CERCO 2085 UV lens adapted to ultraviolet light and a filter adapted to the spectral signature of the OH* radical. The focal length of the lens is fixed at 98 mm, with an aperture at its maximum: f/2.8. The OH* filter mounted on the UV lens has a maximum transmission of 70% at 310 nm and a 10 nm half-width. The gain of the intensifier was fixed at 3V and the gate time of the intensifier was variable, depending on the flame studied, to obtain the best signal dynamics. In the case of the CH4 flame, the OH* radical emits less light than that of hydrogen thus the exposure time of the intensifier had to be increased substantially: 2.5 µs for the CH4 flame instead of 1.6 µs for that of H2, for the same intensifier gain.
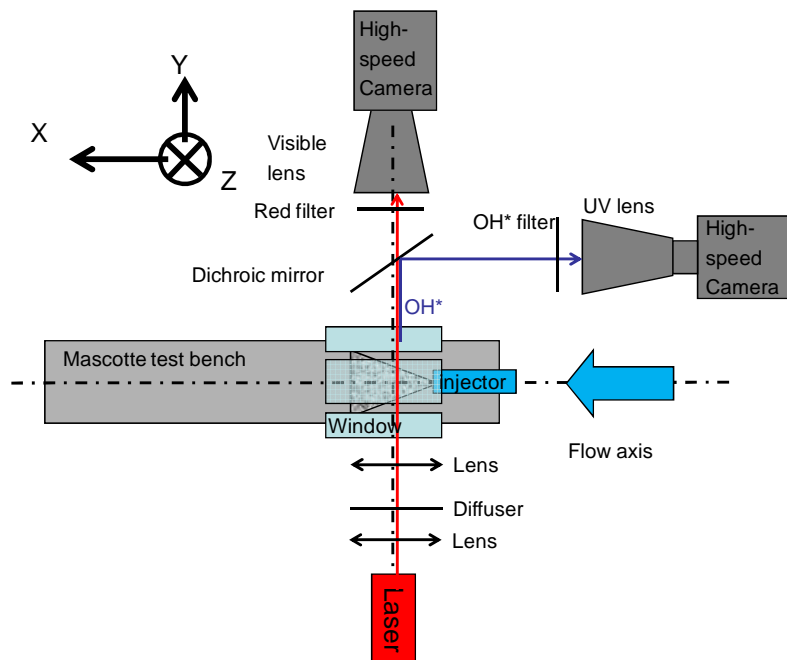
Figure 4: Imaging setup arrangement (top view) with shadowgraphy and chemiluminescence visualizations

OH* emission and shadowgraphy are focused on the same field-of-view, with the same spatial resolution, thanks to the use of a dichroic mirror that separate UV light coming from the OH* chemiluminescence towards the intensified camera and the visible light coming from the laser towards the high-speed camera used for shadowgraphy. Moreover

both images are recorded at the same instant, at 1000 frames/s, as the short laser pulse is emitted during the intensifier gate of the intensified camera. Thus both types of images can be directly superimposed as shown in the results section.

2.3 Droplet size measurements

For this droplet-size and velocity measurement test campaign, a PDI system from Artium Technologies Inc. was used. The PDI operating principles are given by Bachalo et al., 2000 and detailed in [13] and [14]. This system measures velocities and sizes of droplets that are considered spherical by the instrument. The optical arrangement of the instrument is schematically shown on Figure 5: in the vertical injection plane (left) and in the horizontal median plane containing the injection axis. The PDI measures simultaneously the diameter and two velocity components (V1 and V2) of liquid oxygen droplets passing through the measurement volume. The measurement volume is shaped by the intersection between four continuous laser beams: two green beams at 532 nm and two blue beams at 491.5 nm placed in a plane perpendicular to that of the green beams. Each pair of beams of the same colour measures a velocity component of the droplet. The drop-size measurement is based on the analysis of the phase shift of the radiations scattered by a droplet passing through the measurement volume, whose signal is recorded by two photodetectors placed behind the receiving lens,.

The PDI receiver is equipped with interference filters in front of each photodetector (blue or green) whose characteristics are a 96% and 98% transmission, and a half-width of 20 nm and 50 nm, respectively for the blue filters (491 nm) and green (532 nm). It is therefore little disturbed by the flame emission, particularly bright in this cryogenic type of combustion. In addition, the red laser source that illuminates the jet for shadowgraphy is also eliminated. Therefore, it allows running simultaneously the high-speed camera that visualizes the LOX jet and the PDI that measures the size and velocities of these same LOX drops. This simultaneity facilitates the implementation of this PDI particle counter, as it is possible to visualize exactly where the PDI measurement volume is located in the image plane and if there are drops, gas or dense LOX jet at this position. In the left image of Figure 1, the green and blue beams of the PDI emitter can be seen together with the red emission of the backlighting source. The PDI receiver, which was positioned at 1 m from the combustion chamber, is visible at the lower right corner of the left image, while the PDI emitter is hidden behind the combustion chamber. The lens of the high-speed camera is visible in the middle, at the top of the image.

The PDI is used in a forward scattering configuration to maximize the light scattered by the LOX drops. The receiver should be placed at a collection angle β which can be set between 20 and 45° (see Figure 5). The optimum collection angle value is 40° to record light scattered by LOX droplets less than 50 μm in size. However, to meet the requirements of the test plan and constraints related to optical access, the angle was finally set at 21.9°. This was the largest possible angle, despite the large windows of the BHF and the position of the injector, off-centered with respect to the median horizontal injection plane of the combustion chamber. In addition, the focal lengths of the PDI emitter and receiver determine the size and velocity ranges. The nominal velocity range is always greater than the one set during the acquisition because the PDI automatically adjusts its velocity range, before each measurement, by taking a reference sample defined by the 500 first detected droplets. The focal length used at the emission is 500 mm and the focal length of the receiver is 1000 mm, which induce a theoretical diameter range of between $1.6 < D < 240.5$ μm. The nominal velocity range is $-176.1 < V1 < 176.1$ m/s for the longitudinal velocity and $-12.3 < V2 < 8.5$ m/s for the radial velocity.

N. Fdida, L. Vingert, Y. Mauriot, L.H. Dorey, M. Théron
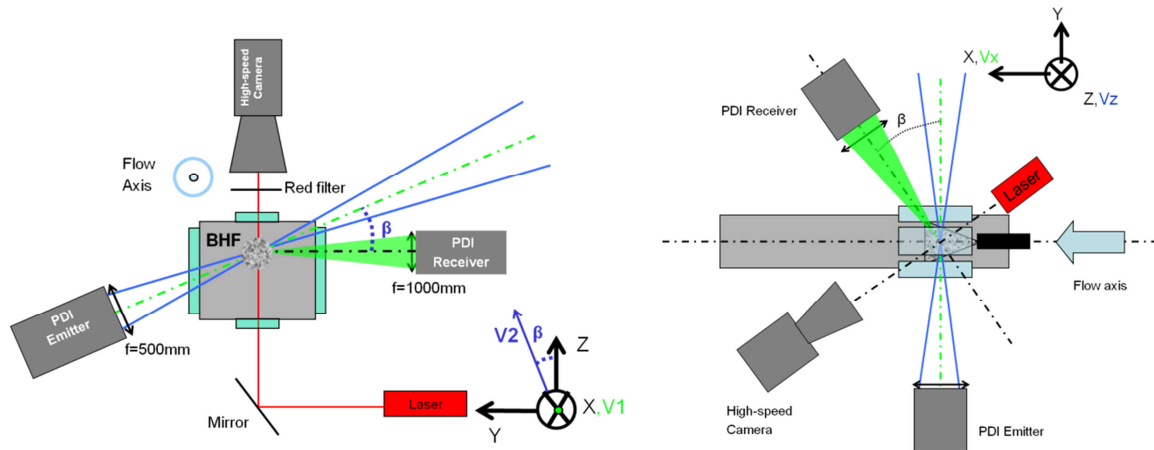
Figure 5: PDI and shadowgraphy arrangement in the vertical injection plane (left) and in the horizontal plane (right)

The droplet diameter measurements with the PDI are based on the knowledge of the refractive index n of liquid oxygen. Johns and Wilheim, 1937 [15] studied the refractive index of several cryogenic liquids and found the value of 1.21 for droplets of liquid oxygen in the air. The gaseous atmosphere in the combustion chamber is composed of a mixture of atomizing gas (hydrogen or methane), oxygen (resulting from the evaporation of the atomized LOX) and a small proportion of helium used to protect the windows from droplet projections. Since these three gases have optical indices close to that of air, it is assumed that the refractive index of liquid oxygen in these experiments is the same as that of liquid oxygen in air. The PDI is a particle counter that counts droplets of liquid oxygen passing through a measuring volume which has the shape of a cylinder with a 1 mm diameter and a length between 25 microns and 500 microns, depending on the slit aperture used in the receiver. The slit width is a parameter which can be automatically optimized by the PDI, however, in practice it is impossible to use this automatic adjustment function of the slit width in the context of such a short measurement period of about 30 seconds. This is why the slit width had to be set before the acquisitions. For this droplet size measurement campaign, the slit size was set at 250 μm. More details on the optical configuration of the PDI and the uncertainties arising from the optical index are presented in [16]. A smaller slit aperture can be useful when the droplet density is high and the presence of multiple droplets in the measurement volume is possible. In our application, the use of a smaller 100 μm slit was tested on several measurement points in very dense zones, where the rate of validated particles was very low, in order to improve the validation rate, but without success. It means that in this low validation rate area, the measurement volume is too close from the LOX jet which traps the light scattered by the droplets. The validation rate is defined by the number of measured droplets over the detected droplets.

The experimental difficulties encountered during the implementation of the PDI are mainly related to the dimensions of the windows. Their large thickness (70 mm) induces multiple reflections, illustrated by the right-hand picture in Figure 1, as well as significant light path differences for the blue laser beams that pass through the windows. Therefore, a specific optical alignment was carried out, taking into account this thickness and the angle of inclination β of the PDI transmitter so that the four laser beams intersect in the same measurement volume. Once this optical alignment for the laser emitter was performed, the second window and the PDI receiver probe was set so that the optical axis was perpendicular to the plane of the window. To ensure a proper alignment, a monodisperse and low density water spray was introduced into the combustion chamber to check that the PDI can measure droplet sizes and velocities. In this case, high validation rates, greater than 90% were obtained with the PDI green beams, providing the droplet size and axial velocity measurements. For the blue channel, which measures only the radial velocity, the validation rates were so low that almost no measurement could be obtained. The differences in light path introduced by the windows thickness are assumed to be the explanation for this lack of measurement.

3. Results

3.1 High-speed images

First, the cryogenic jet flame is illustrated with a large field of view in order to determine the location of the spray. This first phase is essential to locate the PDI measurement points and thus to collect a maximum number of droplets during the duration of the stationary phase of the flow. These large field visualizations are illustrated in Figure 6 by two instantaneous shadowgraph images obtained in both combustion test cases: the LOX/H2 flame on the left and

the LOX/CH4 flame on the right. In the area close to the injector, on the left of each image, the gaseous concurrent jet can be seen, even more contrasted in the case of CH4. This contrast difference highlights the greater density of methane with respect to hydrogen. The time-averaged shadowgraphs are computed from 2000 instantaneous images recorded during the stationary phase of the flow. Then this time-averaged image is binarized in order to obtain the dense core of the LOX jet that is shown in black on Figure 9. The LOX jet seems a little shorter in LOX/CH4 combustion, probably due to the greater J number. Indeed the momentum flux ratio J is known to drive the LOX jet penetration length for this kind of spray [7].
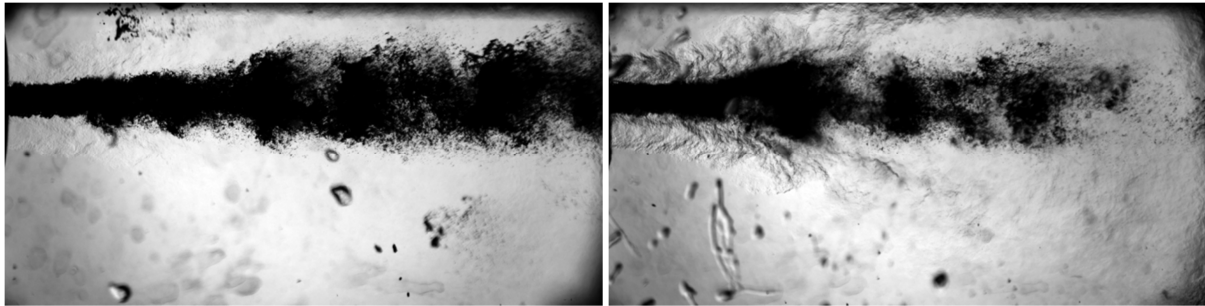
Figure 6: Instantaneous shadowgraph images of the LOX jet flame, with hydrogen (left) and methane (right)

Secondly, two instantaneous OH* emission images are presented on Figure 7 to visualize the structure of the cryogenic flame in the case of the LOX/H2 combustion (left) and LOX/CH4 combustion (right). There are no noticeable differences between the two types of flames during the stationary phase of the flow: both flames seem to be anchored at the tip of the LOX post. The end of the flame cannot be seen inside the viewing windows. The production of OH* emission signal is stronger in the case of LOH/H2 flame as the gate time set on the UV intensifier is about twice shorter than in LOX/CH4, which could be linked to the hotter temperature of the hydrogen flame. From the OH* emission images recorded during the stationary phase of the flow, the time-averaged images (not shown here) have been computed on which the Abel inversion has been applied to extract the front flame in this axisymmetric configuration. The result of the Abel inversion is shown in false colours on Figure 9. The flame opening is similar in both types of flames as the flame full angle has been estimated to be about 20° in both cases. Moreover, as the high-speed cameras are synchronized, simultaneous images of shadowgraphy and chemiluminescence are presented on Figure 6 and Figure 7 for LOX/H2 combustion (left) and for LOX/CH4 combustion (right). Strong spatial correlations are visible between the instantaneous OH* emission images and the corresponding shadowgraphs. Indeed, close to the LOX post, the darkest area in OH* images seem to match the densest areas of the LOX jet in shadow images. Conversely, there is no more dense LOX jet or large liquid elements in the brightest areas of OH* signal.
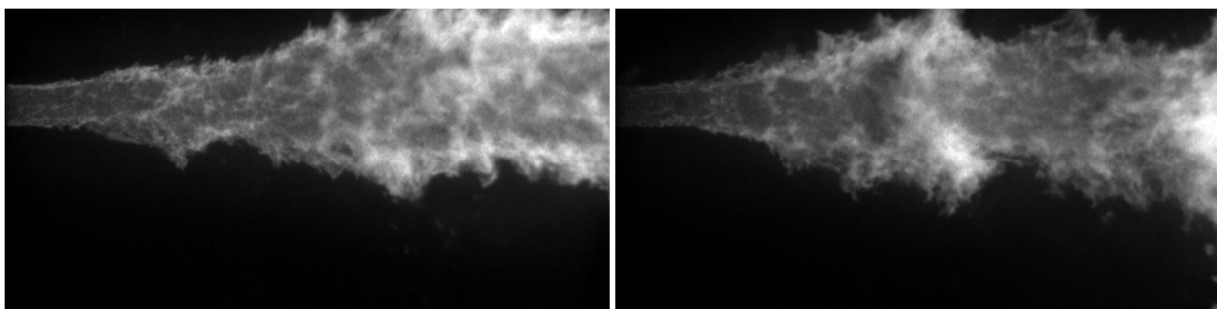
Figure 7: Instantaneous OH* images of the LOX jet flame, with hydrogen (left) and methane (right)

These complementary features of both kinds of images are even clearer when instantaneous OH* emission images and shadowgraphs are superimposed. Examples of digital superimpositions of the LOX jet and instantaneous OH* emission images of Figure 6 and Figure 7 are shown in Figure 8. The instantaneous shadowgraph of the LOX jet image on Figure 6 is binarized with a threshold level chosen to reveal only the darkest elements, that are usually the largest liquid elements; the resulting binary image is thus superimposed to the instantaneous OH* emission image, recorded at the same instant, in false colors. It is found that areas showing low OH* emission signal agrees fairly well to areas showing large liquid elements, that are less prone to burn than smaller droplets. Moreover, the sinuosity

N. Fdida, L. Vingert, Y. Mauriot, L.H. Dorey, M. Théron

at the LOX jet interface matches well the OH* zones situated at the periphery of the flame. It also turns out that the LOX jet is always confined within the reaction zone represented by the OH* emission signal. The highest PDI validation rates are found in the intermediate zone between the LOX jet limit and the envelope of the reaction zone, probably because of a moderate particle density, due to the the presence of the flame which evaporates the smaller ones.
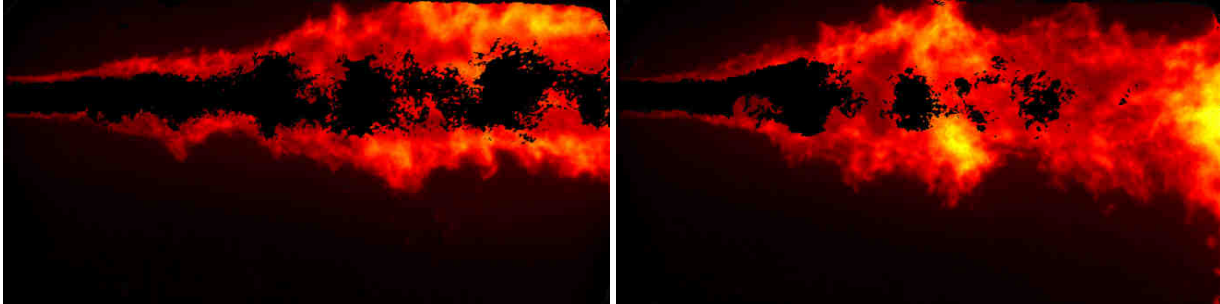
Figure 8: Superimposition of instantaneous shadowgraphs (black) and OH* emission images (colors),
in cases of LOH/H2 (left) and LOX/CH4 (right)

3.2 Droplet size measurements

The complete PDI system (emitter and receiver) is moved by 3-axis translation tables forming a coordinate system linked to the injector location. The origin of the reference coordinate system (0, X, Y, Z), illustrated in Figure 5, is the injector center and the X direction corresponds to the main axis of the flow. In the initial test plan, about fifteen radial positions of PDI measurements were defined in the vertical median plane (X, Z), as shown in Figure 5. In Figure 9, the actual PDI measurement points are symbolized by circles, green when the measured droplet sample is larger than 2000 and red when samples contain less than 2000 droplets (then the measurement is not considered). In Figure 9, the locations of the PDI measurement points are superimposed to the Abel transform of the average OH* image (the false-colors image) and the binarized time-averaged shadowgraph of the LOX jet, in the case of LOX/H2 combustion (left) and in the case of LOX/CH4 combustion (right). Radial lines of PDI points are distributed between the dense zone of the LOX jet (in black in Figure 9) and the outer envelope of the flame front, on either side of the injection axis X. Radially, validation rates vary between a few percent to 40% maximum, the latter value corresponding to a measurement point also previously chosen by Gicquel [5] (surrounded by a yellow circle in Figure 9, left), at position X/DL = 6. The validation rate is linked to the proximity of the PDI measurement volume to the LOX jet interface. Where the measurement volume is too close to the LOX jet, the PDI generally has very low validation rates because most of liquid elements are not spherical and because the density (both optical and in terms of liquid particles per volume) is too important. On the contrary, when the PDI measurement volume is too far from the injection axis, i.e., located radially more than three times the diameter of the injector, there are not enough droplets and even if the validation rates of the measurements of size are good (~ 40%), the number of measured particles is too low to obtain a sufficient number of samples for a robust statistic in the time devoted to the PDI measurement.
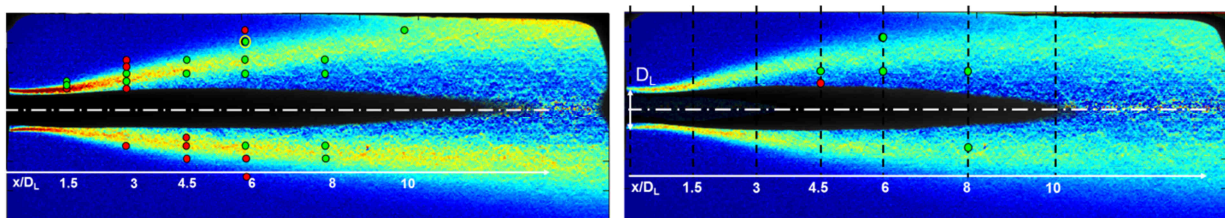
Figure 9: Superimposition of the Abel transform of OH* emission images (color),
the time averaged LOX jet contour (black) and the PDI measurement locations (dots),
in the cases of the LOX/H2 (left) and LOX/CH4 (right) flames.

In the case of CH4 combustion, the validation rates are of the same order than for LOX/H2 combustion (operating point A10), but the number of measured droplets is always lower. This trend could be explained by a lower particle density at a given measurement location. Unfortunately, too few measuring points in CH4 combustion have been

made to conclude. For both fuels (methane and hydrogen), the flame seems to anchor at the LOX post exit. Indeed, the signal of OH* is visible from the exit of the injector located on the left edge of each image.

Examples of raw droplet size histograms measured with PDI at the same location (both axial distance X/DL=6 and radial position) in the LOX jet are shown on Figure 10 for LOX/H2 (in blue) and LOX/CH4 (red) reactive jets. The droplet size distributions look similar in both cases, representative of a monodisperse spray centered on nearly the same diameter. The validation rate is ~15 % for the LOX/H2 and 7.5 % in the LOX/CH4 test case, with respectively 24828 and 3814 measured droplets. The majority of the rejected droplets are due to low signal-to-noise ratio, with a larger rejection rate for the LOX/CH4 case. The second reason for droplet rejection is the non-sphericity of some liquid particles, which is evaluated by the PDI by comparing signals recorded by two different detector pairs. Both propellant test cases show the same level of rejection for non-sphericity.
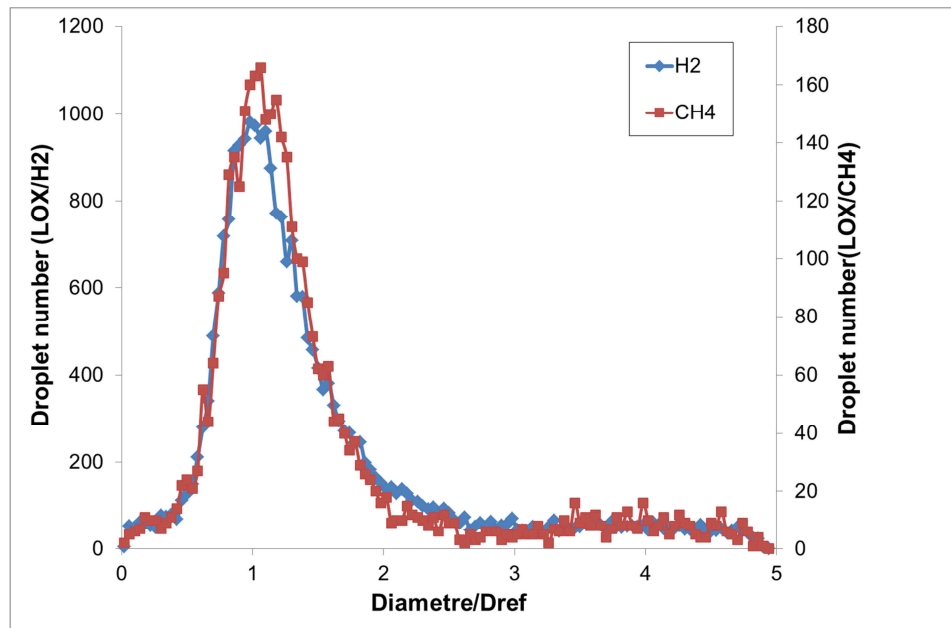
Figure 10: Example of droplet size distribution obtained with PDI at the same location, in the LOX/H2 flame (blue) and LOX/CH4 flame (red).

3. Conclusion

Droplet size and velocity measurements of a LOX spray in burning hydrogen or methane gas were obtained in the atomization zone of the jet flame. The results obtained in the case of hydrogen complete the existing database at the reference operating point A-10 of the MASCOTTE test bench of ONERA [3]. The advantage of the drop-sizing technique by imaging compared to the Doppler Phase Interferometry is its better adaptability to non-spherical particles present in the atomization zone [5]. However, high resolution imaging at the A-10 operating point did not give access to any droplet size result at a close axial distance from the injector, typically less than 6 DL, in the primary atomization zone, whereas such measurements could be carried out with the PDI. Despite a low validation rate, droplet sizes and velocities could be obtained during this experimental test campaign at a distance of 1.5 DL from the LOX post exit. These data are intended to be used for validation of atomization models or initialization of two-phase flow computations. Comparing both fuels, the highest PDI validation rates are obtained in the part of the reaction zone close to the LOX jet, as evidenced by the Abel inversion of OH* emission time-averaged images and the mean shadowgraphs. PDI validation rates appear to be significantly lower in the case of methane than in the case of hydrogen, but additional LOX/CH4 measurements would be required to confirm this point. The droplet size distributions show similar features for both propellants at identical locations, i.e., a monodisperse spray centered on nearly the same droplet size.

During the PDI droplet-size campaign, the temporal resolution of the shadowgraph camera has been increased up to 23 kHz and the spatial resolution was increased too, in order to track the atomization of the LOX jet near the injector exit. Image doublets were obtained with a double exposure acquisition mode to record the liquid structures (including non-spherical ones) in two successive positions, in order to evaluate their velocity with the FOLKI-SPIV

image correlation algorithm [17]. These data are under processing in order to compare the droplets velocity fields obtained with imaging to those obtained by PDI, and to complete the database with non-spherical objects velocity fields.

Acknowledgments

References

[1] Déchelette, A., E. Babinsky, and P.E. Sojka. 2011. Handbook of Atomization and Sprays, 23:479-495.

[2] Murrone, A., N. Fdida, L. Vingert, and C. Le Touze. 2014. Atomization of cryogenic rocket engines coaxial injectors. Modelling aspects and experimental investigations, In: *Space Propulsion 2014*, Köln, Germany.

[3] Habiballah, M., M. Orain, F. Grisch, L. Vingert, and P. Gicquel. 2006. Experimental studies of high-pressure cryogenic flames on the Mascotte test facility, *Combustion Science and Technology*, 178:101-128.

[4] Gicquel, P., and L. Vingert. 2000. Flow investigations of cryogenic sprays in combustion at sub and supercritical conditions, In: *16th Annual Conference on Liquid Atomization and Spray Systems*, 11-13 September, Darmstadt, Germany.

[5] Fdida N., L. Vingert, A. Ristori, and Y. Le Sant. 2016. Drop size and velocity measurements in a cryogenic jet flame of a rocket type combustor using high-speed imaging. *Atomization and Sprays*, 26(5):411-438.

[6] Méry, Y., L. Hakim, P. Scouflaire, L. Vingert, S. Ducruix, and S. Candel. 2013. Experimental investigation of cryogenic flame dynamics under transverse acoustic modulations, *Comptes rendus de la Mécanique*, 341:100-109.

[7] Lasheras, J. and E. Hopfinger, E. 2000. *Annual Review of Fluid Mechanics*, 32:175-308.

[8] Yang, B., F. Cuoco, and M. Oschwald. 2007. Atomization and Flames in LOX/H2- and LOX/CH4-Spray Combustion, *Journal of Propulsion and Power*, 23:763-771.

[9] Cavitar website, https://www.cavitar.com/cavilux-laser-illumination-products/cavilux-smart/

[10] Mayer, W., A. Schik, M. Schäffler, and H. Tamura. 2000. Injection and Mixing Processes in High-Pressure Liquid Oxygen/Gaseous Hydrogen Rocket Combustors, *Journal of Propulsion and Power*, 16(5).

[11] Fiala, T., and T. Sattelmayer. 2017. Comparison Between Excited Hydroxyl Radical and Blue Radiation from Hydrogen Rocket Combustion, *Journal of Propulsion and Power*, Vol. 33, No. 2.

[12] Lux, J., and O. Haidn. 2009. Flame Stabilization in High-Pressure Liquid Oxygen/Methane Rocket Engine Combustion, *Journal of Propulsion and Power*, Vol.25, Issue 1, pp.15-23.

[13] Strakey, P., D. G. Talley, S. V. Sankar, and W. D. Bachalo. 2000. Phase-doppler interferometry with probe-to-droplet size ratios less than unity. I. Trajectory errors. *Applied Optics*, 39(22):3875–86.

[14] Strakey, P., D. G. Talley, S. V. Sankar, and W. D. Bachalo. 2000. Phase-doppler interferometry with probe-to-droplet size ratios less than unity. II. Application of the technique. *Applied Optics*, 39(22):3887-3893.

[15] Johns, H., E., and J.O. Wilheim, The Refractive Indices of Oxygen, Nitrogen and Hydrogen, *Canadian Journal of Research*, 15(7), 1937.

[16] Fdida, N., Y. Mauriot, L. Vingert, A. Ristori, S. Godel, and M. Théron. 2016. Caractérisation de l'atomisation d'un jet d'oxygène liquide assisté par azote gazeux au moyen de diagnostics optiques, In : *CFTL 2016*, Toulouse, France.

[17] Le Besnerais, G., and F. Champagnat, Dense optical flow by iterative local window registration, In: *Proc. of IEEE Int. Conf. on image processing*, ICIP'05, Genova, Italy, pp.137-140, 2005.